ACS Catalysis

Research Article

pubs.acs.org/acscatalysis

# Catalytic Activity of Platinum Monolayer on Iridium and Rhenium Alloy Nanoparticles for the Oxygen Reduction Reaction

Hiroko I. Karan,*[,‡] Kotaro Sasaki,[†] Kurian Kuttiyiel,[†] Carrie A. Farberow,[§] Manos Mavrikakis,[§] and Radoslav R. Adzic[†]

[†]Department of Chemistry, Brookhaven National Laboratory, Upton, New York 11973, United States

[‡]Department of Physical, Environmental and Computer Sciences, Medgar Evers College, The City University New York, 1638 Bedford Avenue, Brooklyn, New York 11225, United States

[§]Department of Chemical & Biological Engineering, University of Wisconsin−Madison, Madison, Wisconsin 53706, United States

Supporting Information

**ABSTRACT:** A new type of electrocatalyst with a core−shell structure that consists of a platinum monolayer shell placed on an iridium−rhenium nanoparticle core or platinum and palladium bilayer shell deposited on that core has been prepared and tested for electrocatalytic activity for the oxygen reduction reaction. Carbon-supported iridium−rhenium alloy nanoparticles with several different molar ratios of Ir to Re were prepared by reducing metal chlorides dispersed on Vulcan carbon with hydrogen gas at 400 °C for 1 h. These catalysts showed specific electrocatalytic activity for oxygen reduction reaction comparable to that of platinum. The activities of $Pt_{ML}/Pd_{ML}/Ir_2Re_1$, $Pt_{ML}/Pd_{2layers}/Ir_2Re_1$, and $Pt_{ML}/Pd_{2layers}/Ir_7Re_3$ catalysts were, in fact, better than that of conventional platinum electrocatalysts, and their mass activities exceeded the 2015 DOE target. Our density functional theory calculations revealed that the molar ratio of Ir to Re affects the binding strength of adsorbed OH and, thereby, the $O_2$ reduction activity of the catalysts. The maximum specific activity was found for an intermediate OH binding energy with the corresponding catalyst on the top of the volcano plot. The monolayer concept facilitates the use of much less platinum than in other approaches. The results with the $Pt_{ML}/Pd_{ML}/Ir_2Re$ electrocatalyst indicate that it is a promising alternative to conventional Pt electrocatalysts in low-temperature fuel cells.

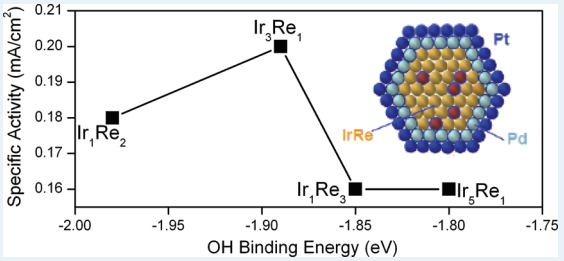


**KEYWORDS:** *oxygen reduction, platinum monolayer, core−shell nanoparticles, electrocatalysis, fuel cells*

## INTRODUCTION

Fuel cells are one of the most promising sources of clean energy, given their uniquely efficient direct energy conversion and the environmentally benign products of their reactions. Extensive research has been conducted on the development of efficient and cost-effective fuel cells; however, their commercial application as a power source in automobiles and residences has yet to be attained, mainly because of technical and economic barriers. During the last two decades, considerable research effort has focused on developing improved electrocatalysts for the oxygen reduction reaction (ORR) at fuel cell cathodes. Platinum is the most efficient monometallic catalyst for the ORR; however, even Pt catalysts lack sufficient activity due to slow ORR kinetics. Insufficient catalysts' stability is caused mainly by Pt dissolution. In the existing catalyst technology, Pt lost to dissolution is compensated for by a relatively high platinum content at the cathode. The associated costs are the obstacle to commercialization of fuel cells,[1−3] which motivates the development of more efficient, lower-cost electrocatalysts.

In meeting the challenges involving the high content of Pt and the insufficient activity and stability of existing electrocatalysts, Pt monolayer ($Pt_{ML}$) electrocatalysts consisting of a single-layer shell of Pt atoms on cores of suitable monometallic or alloy nanoparticles have been developed.[4] This new concept facilitates the design of catalysts with several unique properties: (i) low total Pt content (one monolayer); (ii) complete utilization of Pt, since all atoms are in the surface and directly participate in the reaction; and (iii) tunable activity and stability from the modification of the structural and electronic properties of $Pt_{ML}$ induced by various substrates.[5] These unique features of $Pt_{ML}$ electrocatalysts lead to various possibilities for designing electrocatalysts with specific catalytic properties by choosing appropriate substrates.[5−8] Their mass activity can be more than an order of magnitude higher than that of conventional Pt/C catalysts, and they have improved stability.[5] Early research on this concept demonstrated the effect of the substrate that resulted in a volcano plot with Pt/Pd(111) on the top of the curve as the most active surface.[7] The concept of lateral repulsion between OH on Pt and OH on another metal forming a mixed monolayer with Pt or supporting it has been advanced.[6] Most recent studies using a

Special Issue: Electrocatalysis

Received: November 14, 2011
Revised: March 16, 2012
Published: March 19, 2012

   dx.doi.org/10.1021/cs200592x | ACS Catal. 2012, 2, 817−824

Pt monolayer approach involved varying the shape (tetrahedral,[9] nanowires[10]) and morphology (smooth cores[11]) of supporting nanoparticle cores.

Several other efforts for improving the catalytic properties of Pt and reducing the Pt content in ORR catalysts based on the core−shell approach are exemplified by Pt "skin" catalysts,[12] in which a layer of Pt is formed by surface segregation of Pt in $Pt_3Ni$ alloy and in some bimetallic dealloyed catalysts.[13] The high activity of the Pt−skin catalyst has been ascribed to the electronic effects of the Ni core.[12] Interesting insight into the role of strain on the catalytic properties was reported for a Pd monolayer deposited at underpotentials (UPD) at several single crystal surfaces[14] in formic acid oxidation and hydrogen evolution reaction.[15] Although limited to Pd, this is an interesting extension of the catalytic effects of UPD adlayers[16] to a noble metal whose coverage does not change with potential in a certain range.

Applying a Pt monolayer clearly contributed to reducing the cost of the catalysts, and these catalysts showed specific activities for the ORR comparable with or higher than conventional Pt electrocatalysts.[4−8,17] Zhang et al. also reported significantly improved ORR efficiency by depositing a Pt monolayer on a core consisting of non-noble metal (Ni or Co)−noble metal (Au or Pd or Pt) alloy nanoparticles.[18] In these catalysts, the noble metal shell protected the non-noble metal core from dissolving in acidic electrolyte and improved the catalytic properties of the Pt monolayer by affecting its electronic properties. Xing et al. reported enhanced ORR activity for catalysts prepared with a Pt monolayer shell on a Pd−Au core,[19] and Sasaki et al. reported that a Pt monolayer on Ir−Fe core shell nanoparticles showed significantly improved electrocatalytic activity and stability.[20] Most recently, Gong et al.[21] reported improved ORR activity for a Pt monolayer and palladium interlayer on an Ir−Co alloy core.

In this study, we have developed a new type of catalyst using nanoparticle alloys of iridium and rhenium as the core with either a platinum monolayer or platinum on a palladium interlayer shell deposited on the core, which, in the case of segregated Ir and Re, can have its own core−shell structure. These core metals were chosen because their electron configurations and d-band centers are in the proximity of Pt,[22] they are adequately stable metals with high melting points and high acid and corrosion resistance, and they are priced lower than Pt. Carbon-supported alloy catalyst nanoparticles of various compositions of iridium and rhenium were prepared. To enhance activities, a palladium or platinum monolayer was deposited on the surface of the iridium and rhenium alloy nanoparticles by galvanic displacement of a Cu monolayer deposited at underpotentials. Catalysts developed by this method were characterized and tested for oxygen reduction activity and performance stability. A density functional theory (DFT) modeling study of a number of Ir−Re alloy compositions as supports for a Pt monolayer and Pt/Pd bilayer provides a fundamental understanding as to why specific Ir−Re compositions in the core of these catalysts can lead to improved ORR rates.

## EXPERIMENTAL SECTION

The reagents, including iridium chloride ($IrCl_3{\cdot}xH_2O$, 52.3% metal content), rhenium chloride ($ReCl_3$, 99.9%), copper(II) sulfate pentahydrate ($CuSO_4{\cdot}5H_2O$), and potassium tetrachloroplatinate ($K_2PtCl_4$), were obtained from Alfa Aesar. Vulcan XC-72R carbon nanopowder (~60 nm) was obtained from Cabot Corp. Perchloric acid (66−71%) was obtained from Fisher Scientific. Nafion, PFSA Dispersion DE 1020, aqueous solution from DuPont or 5% lower aliphatic alcohol solution by Aldrich was used for coating over a glassy carbon electrode surface or added into the aqueous catalyst ink. Millipore distilled water, UV Plus with total organic content control was used to prepare solutions. Research purity grade oxygen gas was obtained from Matheson Tri-Gas, and hydrogen and argon gases were obtained from MG Industries and CGI Gas Technologies, respectively.

The reduction of metal halide was carried out at elevated temperatures in a tube furnace. Potentiostats Volta Lab (model PGZ 402) by Radiometer Analytical, S.A. (Lyon, France) and a BAS Electrochemical Analyzer 100B were used for electrochemical analyses and copper underpotential deposition (UPD) experiments, respectively. For a rotating disk electrode, a modulated speed rotator (Pine Instrument Corp.) was used to control rotation speed. Custom-made electrochemical cells were used for routine electrochemical analyses and copper UPD experiments.

The catalyst particles were deposited on a glassy carbon disk (surface area 0.196 $cm^2$) with a Pt ring (Pine Instruments, Grove City, PA). A leak−free Ag/AgCl reference electrode (Cypress Systems Inc., Kansas) which is stored in 3 M NaCl solution was used with a double-junction reference chamber (BAS). A small platinum flag was used as a counter electrode. All the potentials are reported with respect to a reversible hydrogen electrode (RHE). The electrochemical cell, with 20 mL of 0.1 M $HClO_4$ solution, was purged with argon gas for 20−30 min before starting measurements. Oxygen reduction measurements were performed after purging the cell with research purity oxygen gas for 30−40 min to ensure saturation of oxygen in the media. All electrochemical measurements were performed at room temperature.

**Catalyst Synthesis.** The catalyst particles were prepared by mixing desired mole ratios of metals with the carbon nanopowder support. The ratio of the metal mixture to the carbon powder was 3:7 by weight. The aqueous mixture of metal and carbon was sonicated for 30 min, and then the water was evaporated. The dry residue was placed in a quartz boat, which was then placed in a glass tube and purged with argon gas for 20 min and then heated at 400 °C for 1 h under flowing hydrogen gas. The reduced metal catalyst particles were used for subsequent electrochemical analyses and oxygen reduction experiments.

Twenty nanomoles of aqueous mixture of the catalyst particles was sonicated briefly (less than 20 min), and 15−20 $\mu$L (~0.2 mg/$cm^2$) of the ink produced was placed on the surface of a glassy carbon ring electrode. The electrode surface was dried under vacuum and then coated by 5 $\mu$L of 0.025% Nafion (diluted with distilled water from a 5% Nafion solution by Aldrich) and dried under vacuum to evaporate the water from the surface. Cyclic voltammograms (CVs) of the initial catalysts were taken, and then the electrocatalysts were prepared by depositing Pd or Pt monolayers on the iridium and rhenium alloy substrate by galvanic displacement of an underpotentially deposited Cu monolayer by Pd or Pt. This rather straightforward method has been reported by the authors elsewhere.[5,23,24] Copper UPD was performed in a custom-made multiple chamber cell using 50 mM $CuSO_4{\cdot}5H_2O$ in 50 mM $H_2SO_4$, 1 mM $PdCl_2$ in 50 mM $H_2SO_4$, and 1 mM $K_2PtCl_4$ in 50 mM $H_2SO_4$ solutions. The 50 mM $CuSO_4{\cdot}5H_2O$ in 50 mM $H_2SO_4$ solution as well as Pd and Pt solutions were purged by


dx.doi.org/10.1021/cs200592x | ACS Catal. 2012, 2, 817−824

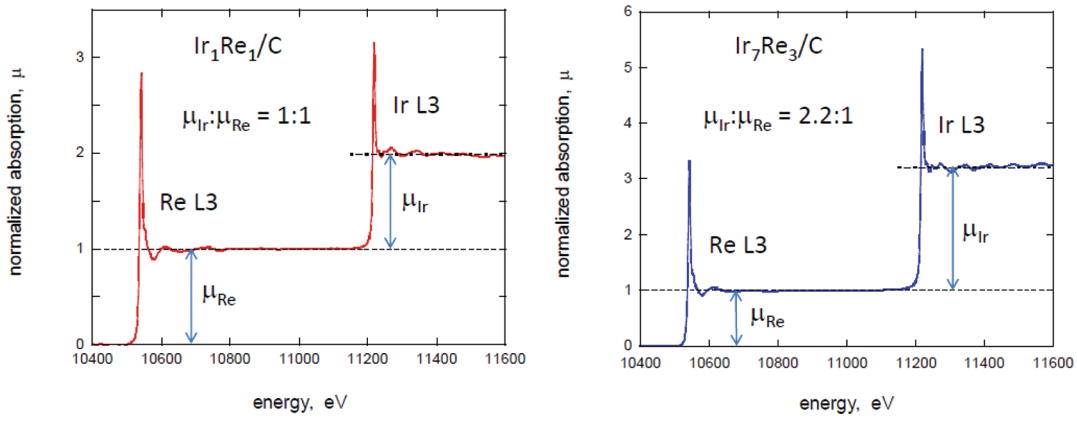


**Figure 1.** XAS results of Re L3 edge (10 535 eV) and Ir L3 edge (11 215 eV) from $Ir_1Re_1/C$ and $Ir_7Re_3/C$ catalysts prepared by hydrogen reduction of the metal chloride mixtures at 400 °C.

argon gas for 20−30 min before starting the Cu UPD and during the displacement experiments.

After the deposition of Pd and Pt monolayers, voltammetry was used to determine the quantity of Pt deposited on the core nanoparticles from the change associated with hydrogen adsorption. Subsequently, kinetic measurements of the ORR were carried out. All electrochemical experiments except oxygen reduction were performed in an Ar gas environment.

The catalysts were characterized electrochemically and using X-ray diffraction (XRD), transmission electron microscopy (TEM), and X-ray absorption near edge structure (XANES) spectroscopy. In situ XANES measurements were conducted using an electrochemical cell designed for data acquisition in fluorescence transmission mode. The compartments for the working and counter electrodes were separated by a proton exchange membrane (Nafion 117, Du Pont Chemical Co., Wilmington, DE). The experiments were carried out at the beamline X-19A at the National Synchrotron Light Source. TEM measurements were performed using a JEOL 2100F (STEM/EDX) equipped with a Schottky field emission source operated at 300 keV, an ultrahigh-resolution objective lens pole piece, an energy dispersive X-ray spectrometer, and a post column Gatan imaging filter. Powder samples were dispersed on a Cu mesh grid coated with a lacey amorphous carbon film.

**Density Functional Theory Calculations.** Periodic, DFT calculations of OH binding energies on appropriately selected model surfaces were performed with the PW91-GGA exchange-correlation functional using the DACAPO total energy code.[25,26] The bulk structures of the alloys were determined from the stable ordered phases defined by the Ir−Re phase diagram:[27,28] $Ir_1Re_2$ and $Ir_1Re_3$ were modeled as hexagonal close-packed (hcp) alloys, and $Ir_3Re_1$ and $Ir_5Re_1$ were modeled as face-centered cubic (fcc) alloys. For the hcp bulk alloys, the calculated optimized lattice constants were 2.77 and 2.76 Å and $c/a$ ratios were 1.57 and 1.59 for $Ir_1Re_2$ and $Ir_1Re_3$, respectively. The optimized lattice constants for the $Ir_3Re_1$ and $Ir_5Re_1$ fcc bulk alloys were 3.86 and 3.92 Å, respectively. The closest-packed (111) and (0001) facet of the catalysts were modeled with a $2\sqrt{3} \times 2\sqrt{3}$ unit cell, corresponding to an adsorbate (OH) coverage of 1/12 ML. The metal slabs consist of five total layers, with the top three layers relaxed and five equivalent layers of vacuum between successive slabs. Nilekar and Mavrikakis elsewhere provide additional technical details for these calculations.[29]

## RESULTS AND DISCUSSION

**Characterization of Carbon-Supported Iridium−Rhenium Alloy Nanoparticles.** Carbon supported iridium−rhenium alloy nanoparticles with several different molar Ir/Re ratios (5:1, 3:1, 7:3, 2:1, 1:1, 1:2, 3:7 and 1:3) were prepared by reducing 3:7 mixtures of desired molar ratios of metal chlorides and Vulcan carbon (average diameter of 60 nm) by hydrogen gas at 400 °C for 1 h. The XRD of the resultant nanoparticles showed broad bands of iridium and rhenium (Supporting Information Figure S1 and Figure S2), which appear to indicate the amorphous state of these nanoparticles. Iridium in an alloy with rhenium should surface-segregate, as predicted by a computational study of alloy surface segregation energies.[26] For very small particles (3 nm), such a layer may not produce sufficient XRD signal. The peaks for H adsorption and Cu UPD in voltammetry curves are similar to those obtained for Ir nanoparticles, but have no similarity with Re (Supporting Information, Figure 3S). Thus, voltammetry provides a strong support for the surface segregation of Ir.

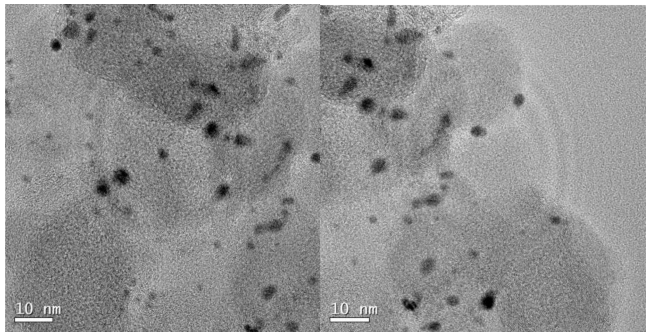


**Figure 2.** TEM images of $Ir_7Re_3/C$ catalyst. The average size of the catalyst particle is 3.3 ± 1 nm.

X-ray absorption spectroscopy (XAS) measurements showed that the metal alloy nanoparticles (1:1 and 7:3 molar Ir/Re ratio) retained the original composition of metals after reducing the metal chlorides (Figure 1). On the basis of TEM images (Figure 2), the average size of these nanoparticles was 3.3 ± 1 nm.

**Pt (Pd) Monolayer Deposition on Carbon-Supported Ir−Re Nanoparticles.** Pt monolayer ($Pt_{ML}$) or Pd monolayer ($Pd_{ML}$) plus $Pt_{ML}$ deposition on the carbon-supported Ir−Re nanoparticles was performed by galvanic displacement of a Cu


dx.doi.org/10.1021/cs200592x | ACS Catal. 2012, 2, 817−824

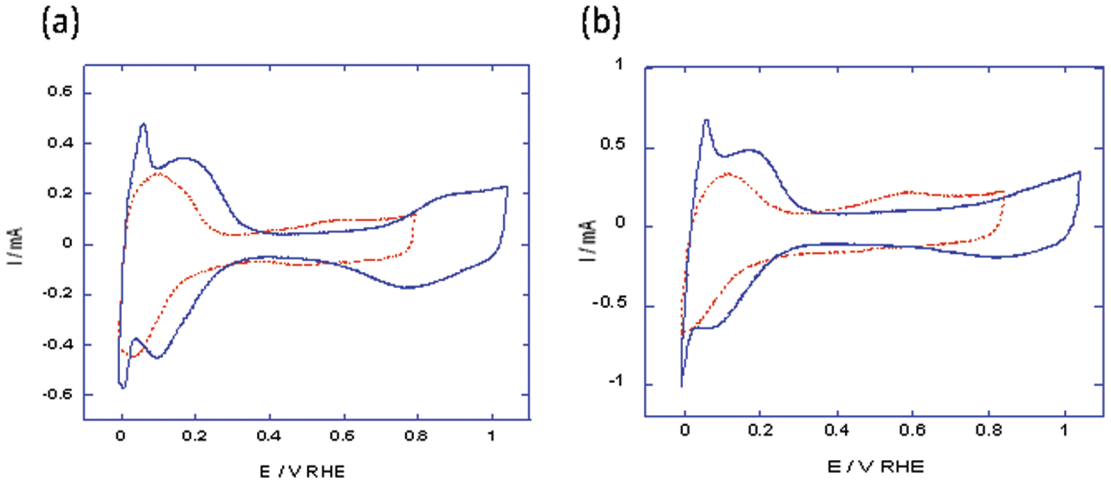


**Figure 3.** Voltammetry curves for (a) $Ir_7/Re_3/C$ and (b) $Ir_1Re_1/C$ alloy nanoparticles (dotted red lines) and the same nanoparticles after deposition of two layers of Pd and Pt monolayer (solid blue lines) in deaerated 0.1 M $HClO_4$. Sweep rate: 10 mV/s.

**Table 1. Half-Wave Potentials ($E_{1/2}$) of the ORR on $Pt_{ML}$, $Pd_{interlayer}$ and $Pt_{ML}$, and Two $Pd_{interlayer}$ and $Pt_{ML}$ for the Various Mole Ratios of Ir−Re/C Core**

| | | $E_{1/2}$ mV, RHE | | |
|---|---|---|---|---|
| catalysts | Ir−Re mole ratio | $Pt_{ML}$/Ir−Re/C | $Pt_{ML}/Pd_{ML}$/Ir−Re/C | $Pt_{ML}$/Pd 2layers/Ir−Re/C |
| Ir−Re/C | 5:1 | 837 | 848 | |
| | 3:1 | 879 | 857 | 859 |
| | 2.3:1 | 821 | 882 | 888 |
| | 2:1 | 879 | 890 | 893 |
| | 1:1 | 802 | | 859 |
| | 1:2 | 765 | 803 | |
| | 1:2.3 | | 831 | 761 |
| | 1:3 | 812 | 814 | |
| Pt/C | | 855 (ref 10) | | |

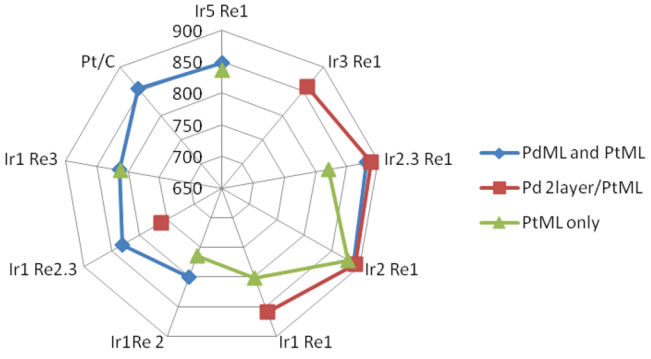


**Figure 4.** Comparison of half-wave potentials of ORR at 1600 rpm for different shells ($Pt_{ML}$, $Pd_{ML}$ and $Pt_{ML}$, and two Pd interlayers and $Pt_{ML}$) on Ir−Re cores with various mole ratios of Ir to Re obtained in $O_2$-saturated 0.1 M $HClO_4$. Sweep rate: 10 mV/s.

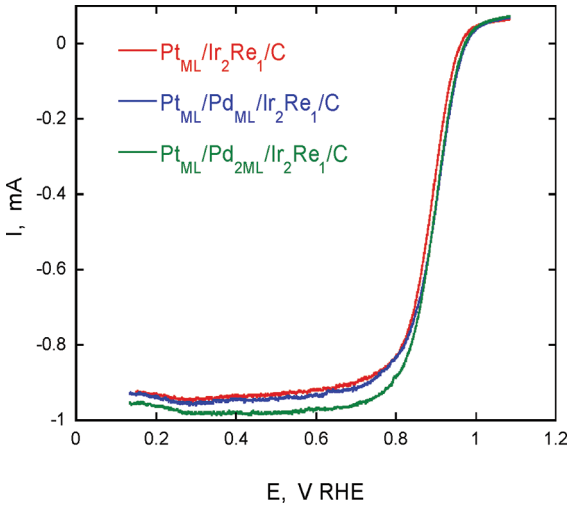


**Figure 5.** Rotating disk electrode measurements of ORR on $Pt_{ML}/Ir_2Re_1/C$, $Pt_{ML}/Pd_{ML}/Ir_2Re_1/C$, and $Pt_{ML}/Pd_{2\,ML}/Ir_2Re_1/C$ catalysts at 1600 rpm in $O_2$-saturated 0.1 M $HClO_4$. Sweep rate: 10 mV/s.

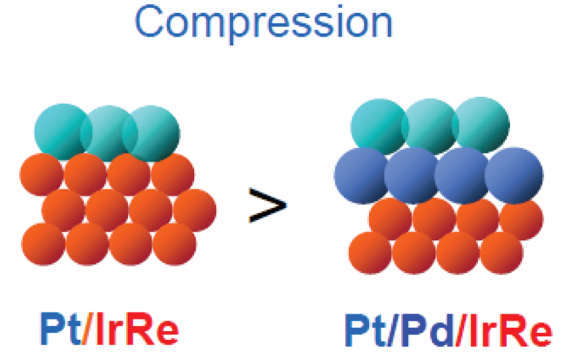


**Figure 6.** Schematic illustrations of $Pt_{ML}$, and $Pd_{ML}$, and $Pt_{ML}$ on the Ir−Re alloy cores.

UPD monolayer. This deposition method via Cu UPD has been discussed in detail in the authors' previous reports.[4−9] The UPD of Cu on the working electrode was carried out in 50 mM $CuSO_4$ in 50 mM $H_2SO_4$ at ~400 mV. The electrode was immersed and placed in either 1.0 mM $K_2PtCl_4$ in 50 mM $H_2SO_4$ or 1.0 mM $PdCl_2$ in 50 mM $H_2SO_4$ for 3 min to deposit Pt or Pd monolayer by replacing Cu.

Figure 3a and b shows the CVs of the initial $Ir_7Re_3/C$ and $Ir_1Re_1/C$ nanoparticles (dotted line) and after depositing two layers of Pd and a Pt monolayer (solid line), respectively, which clearly indicate Pt monolayer deposition on $Ir_7Re_3/C$ and $Ir_1Re_1/C$ nanoparticle surfaces. The Pt concentrations deposited on carbon-supported Ir−Re nanoparticles averaged


dx.doi.org/10.1021/cs200592x | ACS Catal. 2012, 2, 817−824

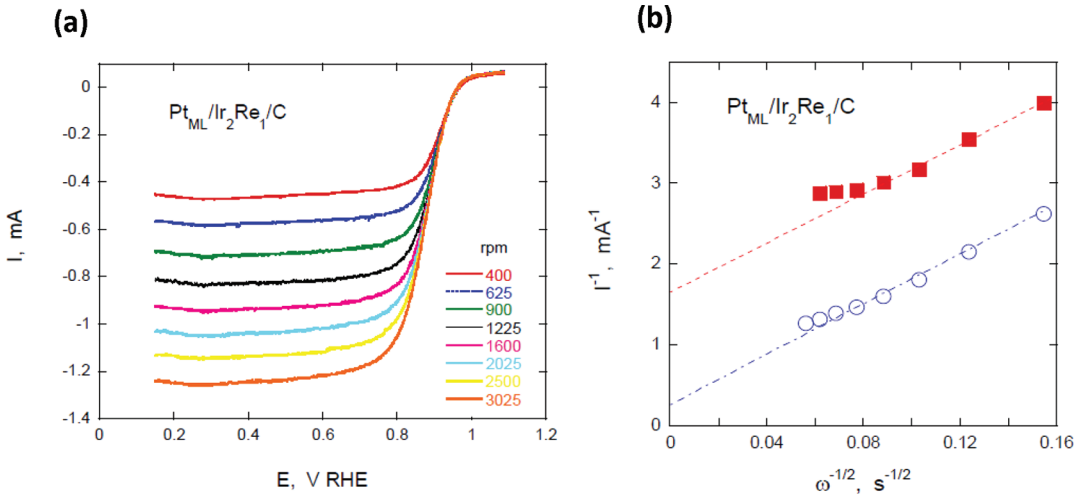


**Figure 7.** (a) RDE measurements of the ORR on $Pt_{ML}/Ir_2Re_1/C$ catalyst as a function of rotation rate. (b) Koutecky–Levich plot ($I^{-1}$ vs $\omega^{-1/2}$) for $Pt_{ML}/Ir_2Re_1/C$ at potentials 0.90 V (■) and 0.85 V ($o$) based on the data obtained in Figure 7a in an $O_2$-saturated 0.1 M $HClO_4$. Sweep rate: 10 mV/s.

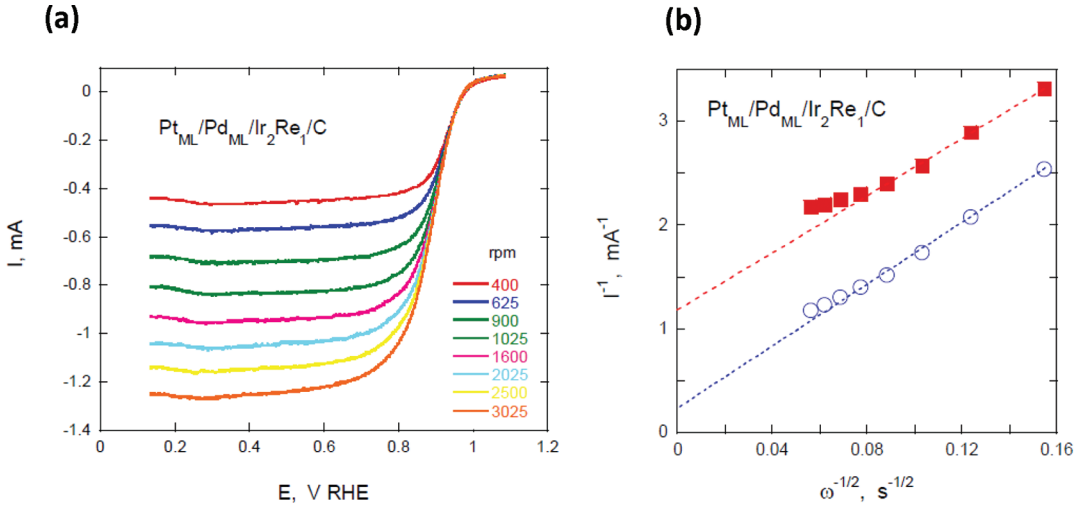


**Figure 8.** (a) RDE measurements of ORR on $Pt_{ML}/Pd_{ML}/Ir_2Re_1/C$ catalyst as a function of rotation rate. (b) Koutecky–Levich plot for $Pt_{ML}/Pd_{ML}/Ir_2Re_1/C$ at potentials 0.90 V (■) and 0.85 V ($o$) based on the data obtained in Figure 8a in an $O_2$-saturated 0.1 M $HClO_4$. Sweep rate: 10 mV/s.

$2.8 \times 10^{-3}$ mg for $Ir_7Re_3$ and $1.4 \times 10^{-3}$ mg for $Ir_1Re_1$. The efficiency of the galvanic displacement of a Cu UPD monolayer by Pt and the evidence of obtaining one monolayer of Pt (i.e. one-to-one correspondence between Cu coverage and Pt coverage) was verified in our earlier publications for properly performed experiments.[17,30,31] Pt coverages lower than one monolayer usually result from a partial loss of Cu coverage if the displacement is not $O_2$-free. Pt coverages greater than one monolayer may occur if a partial displacement of low-coordination Pd atoms takes place during long exposures to Pt solution.

Recently Gokcen et al. studied the stoichiomentry of Pt submonolayer deposition on a Au crystal via surface-limited redox replacement reaction.[32] Their results indicated that under specific experimental conditions, oxidation of Cu UPD adatoms to Cu(I) is thermodynamically more favorable than their oxidation to Cu(II) in the presence of $\{PtCl_6\}^{2-}$, and hence, the results indicated that four Cu UPD adatoms were replaced by one Pt adatom. Cheng et al. reported the substrate dependence of Pt monolayer deposition by Cu UPD on Au structures grown on carbon fiber paper.[33] Their results showed that an equivalent of two monolayers is the low loading limit of Pt on Au. Low loading of Pt causes low activity and durability due to the presence of cationic Pt. These studies add to the understanding of metal deposition via Cu UPD; however, they may not be directly applicable to our current system because of different experimental conditions and substrate properties.

**Oxygen Reduction.** Table 1 summarizes the half-wave potentials of ORR polarization curves of $Pt_{ML}$ or $Pd_{ML}$ and $Pt_{ML}$ shells on different compositions of Ir–Re/C core in oxygen-saturated $HClO_4$ at 1600 rpm. The results show that when the Ir/Re mole ratio is ~2:1, half-wave potentials of the ORR polarization curves appear to be the highest. When the mole ratio of either Ir or Re increases, ORR efficiency appears to decrease (Figure 4). Since Re is much less expensive than Ir, increasing the Re fraction in Ir–Re alloys will reduce the cost of the catalysts. Our results show that the optimum molar ratio of Ir/Re in the catalyst is 2:1. To compare the effect of the shell structure on the ORR efficiency, different shell structures were also studied.

Figure 5 shows the ORR curves of $Pt_{ML}$, $Pd_{ML}$, and $Pt_{ML}$, and two layers of Pd and one $Pt_{ML}$ on the $Ir_2Re_1$ core using a


dx.doi.org/10.1021/cs200592x | ACS Catal. 2012, 2, 817–824

**Table 2. Pt Mass, Platinum Group Metal (PGM) Mass and Specific Activities of $Pt_{ML}$, $Pt_{ML}$ and one $Pd_{interlayer}$, and $Pt_{ML}$ and two $Pd_{interlayer}$ at 0.9 V/RHE for the Various Mole Ratios of the Ir−Re/C Core**

| | | Pt mass activity (A/mg) | PGM mass activity (A/mg) | specific activity ($\mu$A/cm$^2$) |
|---|---|---|---|---|
| $Ir_5Re_1$/C | | | | |
| | *a* | 0.19 | 0.05 | 160 |
| | *b* | 0.36 | 0.1 | |
| $Ir_3Re_1$/C | | | | |
| | *a* | 0.35 | 0.11 | 200 |
| | *b* | 0.45 | 0.14 | |
| $Ir_7Re_3$/C | | | | |
| | *c* | 0.44 | 0.13 | 201 |
| $Ir_2Re_1$/C | | | | |
| | *a* | 0.38 | 0.12 | 161 |
| | *b* | 0.60 | 0.18 | 274 |
| | *c* | 0.59 | 0.18 | 246 |
| $Ir_1Re_2$/C | | | | |
| | *a* | 0.16 | 0.05 | 180 |
| | *b* | 0.43 | 0.13 | |

[a] $Pt_{ML}$. [b] $Pt_{ML}$ and one Pd interlayer. [c] $Pt_{ML}$ and two Pd interlayers.

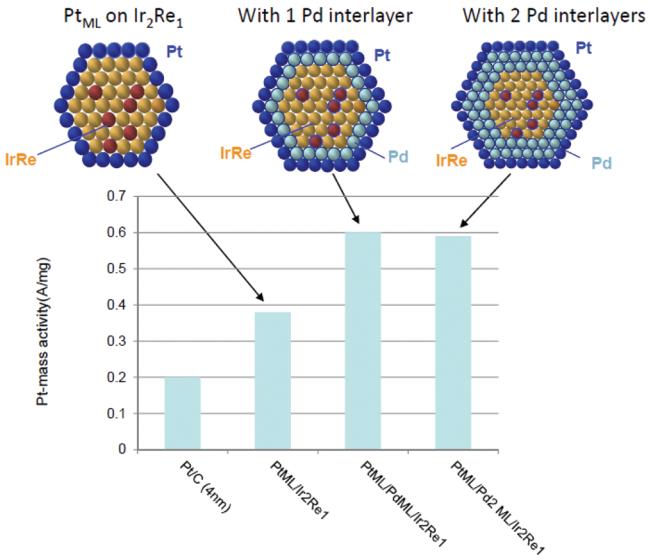


**Figure 9.** Comparison of Pt mass activities for an $Ir_2Re_1$/C core with different shells ($Pt_{ML}$, $Pt_{ML}$ and $Pd_{ML}$, and $Pt_{ML}$ and $Pd_{2ML}$). Corresponding models of cross sections of nanoparticles are also given.

rotating disk electrode (RDE) in oxygen-saturated 0.1 M $HClO_4$ solution at 1600 rpm. Significant activity of the electrocatalysts can be inferred from a high onset potential (~1.0 V) of oxygen reduction and high half-wave potentials. The results show that placing a Pd interlayer improves the activity of the catalysts. It is expected that when $Pt_{ML}$ is directly deposited on the Ir−Re core, Pt atoms will have strong compressive strain due to lattice compression, which adversely affects the Pt ORR catalytic activity. It is likely that the excessive contraction comes from an Ir surface, which is formed by its surface segregation, as discussed above. The Pd interlayer moderates the contraction of the Pt monolayer and precludes the adverse effect on the catalytic activity of Pt (Figure 6).

Figure 7a shows the ORR measurements on $Ir_2Re_1$ catalyst coated with a monolayer of Pt using a RDE in an $O_2$-saturated

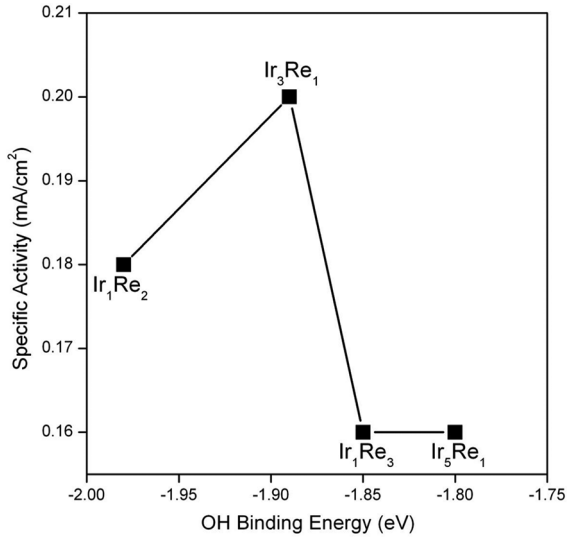


**Figure 10.** Specific activities of the $Pt_{ML}/Pd_{ML}$/Ir−Re alloy catalysts plotted against the calculated OH binding energy. The labels indicate the Ir−Re alloy composition of each data point.

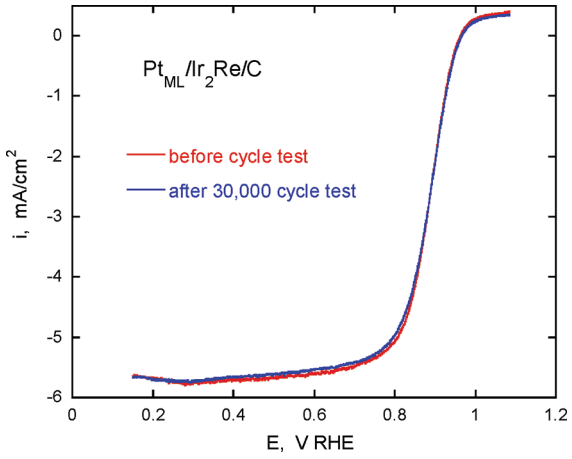


**Figure 11.** Accelerated stability test: the ORR polarization curves on a RDE in oxygen saturated 0.1 M $HClO_4$ at 1600 rpm before and after 30 000 potential cycles from 0.6 to 1.0 V.

0.1 M $HClO_4$ solution at different rotation speeds (400−3025 rpm) at a 10 mV/s sweep rate. Figure 8a shows similar experimental results with the $Ir_2Re_1$/C catalyst coated with $Pd_{ML}$ and then $Pt_{ML}$. The Pt concentrations deposited on the carbon supported $Pt_{ML}$/Ir−Re and $Pt_{ML}/Pd_{ML}$/Ir−Re nanoparticles were 8.2 and 7.35 $\mu$g/cm$^2$, respectively.

Koutecky−Levich plots for $Pt_{ML}/Ir_2Re_1$/C and $Pt_{ML}/Pd_{ML}/Ir_2Re_1$/C based on ORR polarization data obtained in Figure 7a and 8a are shown in Figures 7b and 8b respectively. The linearity and parallelism of these plots indicate first-order kinetics with respect to the concentration of molecular oxygen.[1,5,34] To obtain Pt mass activities (A/mg), the kinetic currents for ORR were determined from the intercepts on $1/j$ at $\omega^{-1/2} = 0$. Table 2 shows Pt mass activities (A/mg) and platinum group metal (PGM) mass activities (A/mg) of different molar compositions of Ir−Re catalysts with $Pt_{ML}$ or $Pt_{ML}$ and one Pd interlayer or $Pt_{ML}$ and two Pd interlayers. In these studies, the $Ir_2Re_1$ core composition showed the highest Pt and PGM mass activities for all three overlayer structures. The Pt and PGM mass activities of $Pt_{ML}/Ir_2Re_1$/C and $Pt_{ML}$/


dx.doi.org/10.1021/cs200592x | ACS Catal. 2012, 2, 817−824

$Pd_{ML}/Ir_2ReML_1/C$ are 0.38 and 0.12 A/mg, and 0.60 and 0.18 A/mg at 0.9 V/RHE, respectively. As discussed previously, a Pd interlayer on the $Ir_2Re_1/C$ core enhanced the Pt mass activity of the catalysts compared with that of the catalysts without it. An illustration of the core−shell structure of $Ir_2Re_1$ cores with different shells and a comparison of the their mass activities are shown in Figure 9. These catalysts have higher Pt mass activities than that often observed for a commercial Pt/C catalyst.[30]

The generally accepted four-electron transfer mechanism of oxygen reduction involves O−O bond breaking and O−H bond formation at the catalyst surface. The most effective catalyst is expected to bind oxygen strongly enough to break the O−O bond while binding the OH group only modestly so that OH removal from the catalyst surface by water elimination is also reasonably facile.[25,30]

On the basis of DFT calculations, Nilekar and Mavrikakis[29] investigated correlations between metal d-band center energy or OH binding energy and experimentally determined kinetic currents of electrocatalysts for ORR. Plotting the measured kinetic currents of electrocatalysts, such as transition metal alloys or Pt monolayer core−shell nanoparticles, versus metal d-band center energies or OH binding energies revealed a volcano-type dependence.[6,7] The closer to the peak of the volcano plot a catalyst is situated, the higher the efficiency of kinetics for O−O bond breaking and simultaneous removal of OH from the catalyst surface. Figure 10 shows the specific activity of the Ir−Re alloy catalysts with a $Pt_{ML}$ and Pd interlayer shell on various Ir−Re cores versus the OH binding energy calculated using DFT for the respective close-packed model $Pt_{ML}/Pd_{ML}/Ir-Re$ alloy surfaces.

The OH binding energy calculations support the experimental results discussed above. Whereas $Pt_{ML}/Pd_{ML}/Ir_1Re_2$ binds OH too strongly, making removal of OH via $H_2O$ formation difficult, resulting in poisoning of the catalyst surface by OH, $Pt_{ML}/Pd_{ML}/Ir_1Re_3$ and $Pt_{ML}/Pd_{ML}/Ir_5Re_1$ appear to bind OH too weakly, suggesting weak binding of atomic oxygen and, thus, difficult O−O bond activation. Of the alloys studied using DFT for the purpose of the present study, $Pt_{ML}/Pd_{ML}/Ir_3Re_1$ lies at the peak of the volcano with an intermediate OH binding energy corresponding to a maximum specific activity (Figure 10). Thus, the molar ratio of Ir to Re in the catalyst influences the binding strength of adsorbed OH and, thereby, the ORR activity of the catalysts. The systems considered using DFT have been restricted to those that are stable, ordered phases as defined by the Ir−Re bulk alloy phase diagram.[27,28] Unfortunately, we cannot comment on the OH binding energy on the optimum catalyst identified in the experiments, $Pt_{ML}/Pd_{ML}/Ir_2Re_1/C$. However, from those systems in which both the experimental and theoretical analysis has been completed, we note the agreement between the experimental and theoretical results in identifying $Pt_{ML}/Pd_{ML}/Ir_3Re_1$ as the best of those catalysts. This result demonstrates that the OH binding energy works well as a reactivity descriptor for ORR, as demonstrated previously for a number of other systems.[6,7,9]

**Performance Stability of the Catalysts.** An accelerated stability test for the $Pt_{ML}/Pd_{ML}/Ir_2Re_1$ catalyst was performed using a rotating disk electrode in a 0.1 M $HClO_4$ solution at room temperature. Figure 11 shows the ORR polarization curves at 1600 rpm before and after 30 000 potential cycles from 0.6 to 1.0 V. After 30 000 cycles, the half-wave potential of the ORR polarization curve resumed at almost the original level when the cell medium was changed to fresh electrolyte and was tested for ORR. This indicates good stability and durability of the $Pt_{ML}/Pd_{ML}/Ir_2Re_1$ catalyst at ambient temperature under the accelerated test conditions.

## SUMMARY

New compositions of core−shell ORR catalysts were prepared by layering palladium and platinum monolayers on various molar ratios of iridium to rhenium mixed-core nanoparticles supported by Vulcan carbon. These catalysts are durable and acid resistant and exhibit electrocatalytic activity for oxygen reduction comparable to platinum. In the case of $Pt_{ML}/Pd_{ML}/Ir_2Re_1$, $Pt_{ML}/Pd_{2layers}/Ir_2Re_1$, and $Pt_{ML}/Pd_{2layers}/Ir_7Re_3$ catalysts, the ORR kinetics were, in fact, better than that of monometallic platinum, and mass activities exceeded the 2015 US Department of Energy target level (0.44 A/mg). Applying the Pt and Pd monolayer on the core metals using the Cu-UPD technique requires the use of much less platinum. According to our DFT calculations, Ir and Re mixed-metal cores contribute to decreasing OH poisoning of Pt. The catalyst with an $Ir_2Re_1$ core composition showed the highest ORR kinetics of those tested. When the mole ratio of Ir to Re at the core deviated from ∼2:1, the ORR efficiency decreased. The Pd interlayer in the shell enhanced catalyst activity. These factors appear to affect the OH binding energy such that an intermediate OH binding energy corresponding to a maximum in the catalyst activity could be achieved. The accelerated test involving 30 000 potential cycles shows the remarkable stability of these catalysts. The results show that $Pt_{ML}/Pd_{ML}/Ir_2Re_1$ catalysts are a promising alternative to pure Pt ORR catalysts in low-temperature fuel cells.

## ASSOCIATED CONTENT

### Supporting Information

Figures S1, S2, and S3. This material is available free of charge via the Internet at http://pubs.acs.org.

## AUTHOR INFORMATION

### Corresponding Author

*E-mails: (H.I.K.) hiroko@mec.cuny.edu; (R.R.A.) adzic@bnl.gov.

### Notes

The authors declare no competing financial interest.

## ACKNOWLEDGMENTS

This work is supported by U.S. Department of Energy, Basic Energy Sciences, Divisions of Chemical and Material Sciences, Material Sciences and Engineering Division, under the Contract No. DE-AC02-98CH10886. Work at UW−Madison was supported by DOE-BES, Chemical Sciences. C.A.F. thanks the NSF for a Graduate Research Fellowship under Grant No. DGE-0946806. Research was performed using supercomputing resources at EMSL, a national scientific user facility located at Pacific Northwest National Laboratory; the National Center for Computational Sciences (NCCS) at Oak Ridge National Laboratory; and the National Energy Research Scientific Computing Center (NERSC). EMSL is sponsored by the U.S. Department of Energy's Office of Biological and Environmental Research. NCCS and NERSC are supported by the Office of Science of the U.S. Department of Energy under Contracts Nos. DE-AC05-00OR22725 and DE-AC02-05CH11231, respectively. H.I.K. acknowledges a sabbatical fellowship by Medgar Evers College, The City University of

New York, and the sabbatical program sponsored by the office of Educational Programs at Brookhaven National Laboratory.

## REFERENCES

(1) Adzic, R. R. In *Electrocatalysis*; Lipkowski, J., Ross, P. N., Eds.; Wiley-VCH: New York, NY, 1998; pp 197−242.
(2) Markovic, N. M.; Schmidt, T. J.; Stamenkovic, V.; Ross, P. N. *Fuel Cells* **2001**, *1*, 105−116.
(3) Morozan, A.; Jousselme, B.; Palacin, S. *Energy Environ. Sci.* **2011**, *4*, 1238−1254.
(4) Adzic, R. R.; Zhang, J.; Sasaki, K.; Vukmirovic, M. B.; Shao, M.; Wang, J. X.; Nilekar, A. U.; Mavrikakis, M.; Valerio, J. A.; Uribe, F. *Top. Catal.* **2007**, *46*, 249−262.
(5) Zhang, J.; Mo, Y.; Vukmirovic, M. B.; Klie, R.; Sasaki, K.; Adzic, R. R. *J. Phys. Chem. B* **2004**, *108*, 10955−10964.
(6) Zhang, J.; Vukmirovic, M. B.; Sasaki, K.; Nilekar, A. U.; Mavrikakis, M.; Adzic, R. R. *J. Am. Chem. Soc.* **2005**, *127*, 12480−12481.
(7) Zhang, J.; Vukmirovic, M. B.; Xu, Y.; Mavrikakis, M.; Adzic, R. R. *Angew. Chem., Int. Ed.* **2005**, *117*, 2170−2173.
(8) Shao, M. H.; Huang, T.; Liu, P.; Zhang, J.; Sasaki, K.; Vukmirovic, M. B.; Adzic, R. R. *Langmuir* **2006**, *22*, 10409−10415.
(9) Gong, K.; Vukmirovic, M. B.; Ma, C.; Zhu, Y.; Adzic, R. R. *J. Electroanal. Chem.* **2011**, *662*, 213−218.
(10) Koenigsmann, C.; Santulli, A. C.; Gong, K.; Vukmirovic, M. B.; Zhou, W.-P.; Sutter, E.; Wong, S. S.; Adzic, R. R. *J. Am. Chem. Soc.* **2011**, *133*, 9783−9795.
(11) Cai, Y.; Ma, C.; Zhu, Y.; Wang, J. X.; Adzic, R. R. *Langmuir* **2011**, *27*, 8540−8547.
(12) Stamenkovic, V. R.; Fowler, B.; Mun, B. S.; Wang, G. F.; Ross, P. N.; Lucas, C. A.; Markovic, N. M. *Science* **2007**, *315*, 493−497.
(13) Strasser, P.; Koh, S.; Anniyev, T.; Greeley, J.; More, K.; Yu, C.; Liu, Z.; Kaya, S.; Norlund, D.; Ogasawara, H.; Toney, M. F.; Nilsson, A. *Nat. Chem.* **2010**, *2*, 454−460.
(14) Kibler, L. A.; El-Aziz, A. M.; Hoyer, R.; Kolb, D. M. *Angew. Chem., Int. Ed.* **2005**, *44*, 2−5.
(15) Greeley, J.; Nørskov, J. K.; Kibler, L. A.; El-Aziz, A. M.; Kolb, D. M. *ChemPhysChem* **2006**, *7*, 1032−1035.
(16) Adzic, R. R. In *Advances in Electrochemistry and Electrochemical Engineering*; Gerischer, H., Tobias, C. W., Eds.; John Wiley & Sons: New York, 1984; Vol. *13*, pp 159−260.
(17) Sasaki, K.; Wang, J. X.; Naohara, H.; Marinkovic, N.; More, K.; Inada, H.; Adzic, R. R. *Electrochim. Acta* **2010**, *55*, 2645−2652.
(18) Zhang, J.; Lima, F. H. B.; Shao, M. H.; Sasaki, K.; Wang, J. X.; Hanson, J.; Adzic, R. R. *J. Phys. Chem. B* **2005**, *109*, 22701−22704.
(19) Xing, Y.; Cai, Y.; Vukmirovic, M. B.; Zhou, W.-P.; Karan, H.; Wang, J. X.; Adzic, R. R. *J. Phys. Chem. Lett.* **2010**, *1*, 3238−3242.
(20) Sasaki, K.; Kuttiyiel, K. A.; Su, D.; Adzic, R. R. *Electrocatalysis* **2011**, *2*, 139−142.
(21) Gong, K. P.; Chen, W.-F.; Sasaki, K.; Su, D.; Vukmirovic, M. B.; Zhou, W. P.; Izzo, E.; Perez-Acosta, C.; Hirunsit, P.; Balbuena, P. B.; Adzic, R. R. *J. Electroanal. Chem.* **2011**, *649*, 232−237.
(22) Hammer, B; Nørskov, J. K. *Adv. Catal.* **2000**, *45*, 71−129.
(23) Brankovic, S. R.; Wang, J. X.; Adzic, R. R. *Electrochem. Solid State Lett.* **2001**, *4*, A217−A220.
(24) Brankovic, S. R.; Wang, J. X.; Adzic, R. R. *Surf. Sci.* **2001**, *474*, L173−L179.
(25) Greeley, J.; Nørskov, J. K.; Mavrikakis, M. *Annu. Rev. Phys. Chem.* **2002**, *53*, 319−348.
(26) Hammer, B.; Hansen, L. B.; Nørskov, J. K. *Phys. Rev. B* **1999**, *59*, 7413−7421.
(27) Tylkina, M. A.; Tsyganova, I. A.; Savitskii, E. M. *Russ. J. Inorg. Chem.* **1962**, *7*, 990−996.
(28) Okamoto, H. In *Binary Alloy Phase Diagrams*, 2nd ed.; Massalski, T. B., Ed.; ASM International: Materials Park, OH, 1990; Vol. 3, pp 2345−2346.
(29) Nilekar, A. U.; Marvikakis, M. *Surf. Sci.* **2008**, *602*, L89−L94.
(30) Wang, J. X.; Inada, H.; Wu, L.; Zhu, Y.; Choi, Y.; Liu, P.; Zhou, W.-P.; Adzic, R. R. *J. Am. Chem. Soc.* **2009**, *131*, 17298−17302.
(31) Sasaki, K.; Naohara, H.; Cai, Y.; Choi, Y. M.; Liu, P.; Vukmirovic, M. B.; Wang, J. X.; Adzic, R. R. *Angew. Chem., Int. Ed.* **2010**, *49*, 8602−8607.
(32) Gokcen, D.; Bae, S.-E.; Brankovic, S. R. *J. Electrochem. Soc.* **2010**, *157*, D582−D587.
(33) Cheng, S.; Rettew, R. E.; Sauerbrey, M.; Alamgir, F. M. *ACS Appl. Mater. Interfaces* **2011**, *3*, 3948−3956.
(34) Anastasijevic, N. A.; Vesovic, V.; Adzic, R. R. *J. Electroanal. Chem.* **1987**, *229*, 305−316.